GIDAN MADI MULTI-DISCIPLINARY JOURNAL OF TEACHER EDUCATION (GMMJTE), 3 (1) OCTOBER, 2026
ISSN: 3092-8397; Journal home page: https://www.fcegmmdjte.org.ng

CHARACTERIZATION OF METAL OXIDES, GOLD NANOPARTICLES, AND REDUCED GRAPHENE OXIDE NANOCOMPOSITES FOR ETHANOL SENSING

ABUBAKAR, LAWAL[1], MUSA, MUSTAPHA[2], MANI, SULAIMAN[3] AND MUH'D, S.A.[4]

[1, 3 & 4]Department of Chemistry, Federal College of Education Gidan Madi, Sokoto State.
[2]Department of Chemistry, Shehu Shagari College of Education, Sokoto State.

**Corresponding author lawaligada@gmail.com*

ABSTRACT

The study investigated the structural, morphological, chemical, elemental and textural properties of ZnO–rGO–AuNPs, SnO_2–rGO–AuNPs and NiO–rGO–AuNPs hybrid nanocomposites synthesized using the hydrothermal method. The materials were characterized using field-emission scanning electron microscopy (FESEM), energy-dispersive X-ray spectroscopy (EDX), X-ray diffraction (XRD), Fourier-transform infrared (FTIR) spectroscopy and Brunauer–Emmett–Teller (BET) analysis. FESEM revealed nanoscale particle distributions with varying degrees of agglomeration and surface porosity. EDX identified the principal metal and oxygen elements, although Au was not detected. XRD confirmed the characteristic crystalline phases of ZnO, SnO_2 and NiO, with additional reflections assigned to Au nanoparticles. FTIR identified characteristic metal–oxygen bonds and residual oxygen-containing functional groups, while BET analysis revealed mesoporous structures with surface areas of 12.42, 16.16 and 22.28 m^2/g for ZnO-, SnO_2- and NiO-based composites, respectively. The findings provide useful insights into the physicochemical characteristics of the synthesized materials and their potential suitability for ethanol gas-sensing applications.

ARTICLE INFO
Article History
Received: 25.10.2026
Received in revised form: 17.11.2026
Accepted: 20.11.2026
Published online: 20.11.2026

KEYWORDS
Hybrid nanocomposites, metal oxides, reduced graphene oxide, gold nanoparticles, ethanol sensing

INTRODUCTION

The increasing demand for reliable, sensitive, and selective chemical sensors has stimulated considerable research into the development of nanostructured materials for gas-sensing applications. Ethanol is one of the most widely used volatile organic compounds (VOCs) in industries, laboratories, pharmaceuticals, food processing, alcoholic beverage production, and fuel-related applications. Although ethanol has many useful applications, exposure to high concentrations can pose health and safety risks. In addition, accurate monitoring of ethanol vapour is important in industrial process control, environmental monitoring, breath analysis, and the detection of alcohol levels. Consequently, the development of low-cost, highly sensitive, rapid, and reliable ethanol sensors has become an important area of research (Nagar and Kamathe, 2024; Suresh et al., 2026).

The increasing application of ethanol has therefore created a strong demand for reliable

technologies capable of detecting and monitoring ethanol vapour accurately. Ethanol gas sensors are particularly important in chemical manufacturing plants, fuel-processing facilities, laboratories, food and beverage industries, environmental monitoring systems, and breath-alcohol analysis. In industrial environments, early detection of ethanol leakage can provide an important warning before the vapour reaches hazardous concentrations. Similarly, in environmental and healthcare applications, sensitive detection of low concentrations of ethanol can provide useful information for air-quality assessment and breath analysis. Consequently, the development of gas sensors with high sensitivity, selectivity, rapid response and recovery, low power consumption, and good long-term stability has become an important research area (Li et al., 2024; Wan et al., 2026).

A hybrid nanocomposite can generally be described as a composite material in which different components are incorporated at the nanoscale to obtain synergistic properties that may not be achievable from the individual components alone. The components may include polymers, metals, metal oxides, carbon-based nanomaterials, ceramics, natural materials, or other inorganic and organic constituents. The combination of these materials can result in enhanced mechanical strength, thermal stability, electrical conductivity, optical properties, chemical resistance, catalytic activity, barrier properties, or antimicrobial performance. The properties obtained depend strongly on the nature of the constituent materials, their concentration, particle size, morphology, dispersion, interfacial interaction, and method of synthesis (Shah et al., 2025; Ranga et al., 2026).

The development of hybrid nanocomposites has therefore provided an opportunity to design materials for a wide range of applications. These materials have been investigated for use in energy storage and conversion, environmental remediation, sensors, catalysis, biomedical applications, protective coatings, electronics, packaging, water treatment, and structural materials. However, the performance of a hybrid nanocomposite cannot be adequately understood by considering its individual components alone. The interaction between the different phases and the resulting microstructural features play a major role in determining the final properties of the material. Consequently, proper characterization is an essential aspect of hybrid nanocomposite research (Godja et al., 2024; Machin and Marquez, 2025).

Numerous papers have been published to date for ethanol gas sensing from various sources namely; Metal oxides like ZnO, SnO_2, TiO_2, and Fe_2O_3, hematite (α-Fe_2O_3), and tungsten oxide (WO_3) along with some less commonly used metal oxides with p-type conductivity such as CuO, NiO, and Cr_2O_3 have been commonly employed for gas analyte recognition thanks to their chemical stability, affordable, and ease of synthesis (Wang et al., 24; Heng et al., 2024), Gold nanoparticlesmetal oxides (Chiu et al., 2024; Abdulmunem and Hassan, 2024; Chao et al., 2024), Reduced graphene oxidemetal oxides (Safi and Shah, 2024; An et al., 2024).

With the increased focus on industrial process control, environmental protection, and workplace safety, there is a pressing need for dependable ethanol gas sensors that perform well in ambient conditions. One promising way to deal with these issues is to use hybrid nanocomposites of metal oxides, gold nanoparticles, and rGO. A new generation of ethanol gas sensors that combine high sensitivity, selectivity, low energy consumption, and operational stability can be achieved by addressing these problems. This will ultimately enable safer and more environmentally friendly practices across a variety of applications.

Characterization involves the systematic investigation of the structural, morphological, compositional, thermal, optical, mechanical, and other relevant properties of a material. Through characterization, information can be obtained concerning the chemical composition, crystal structure, particle size, morphology, surface characteristics, functional groups, thermal behaviour, and interaction between the constituent phases of a hybrid nanocomposite (Abdelghani et al., 2025; Tian et al., 2026). Techniques such as Fourier Transform Infrared Spectroscopy (FTIR), X-ray Diffraction (XRD), Scanning Electron Microscopy (SEM), Transmission Electron Microscopy (TEM), Energy-Dispersive X-ray Spectroscopy (EDX), Thermogravimetric Analysis (TGA), Differential Scanning Calorimetry (DSC), and ultraviolet-visible spectroscopy (UV-Vis), among others, may be employed depending on the nature and intended application of the material.

Furthermore, characterization is important for establishing the relationship between the synthesis conditions, structure, and properties of the resulting hybrid nanocomposite. Factors such as synthesis temperature, reaction time, precursor concentration, pH, type of stabilizer, and method of preparation can significantly influence the properties of the final material. Without adequate characterization, it may be difficult to determine how these factors affect particle formation, phase development, morphology, and interfacial interactions (Enferadi et al., 2024; Gambhire et al., 2026). Characterization therefore provides the scientific basis for optimizing the synthesis process and obtaining a material with the desired properties.

Therefore, the aim of this work is to give a comprehensive characterization particularly in establishing the relationship between the physical and chemical properties of the metal oxide-AuNP-rGO hybrid nanocomposite and its ethanol-sensing performance. The morphology and particle distribution observed by FESEM, the surface chemistry revealed by FTIR, the crystal structure identified by XRD, the elemental composition confirmed by EDX, and the surface area and pore characteristics determined by BET which can have potentiality in sensor sensitivity, response time, recovery time, selectivity, and stability. Such information is also essential for optimizing the synthesis conditions and identifying the composition and structure that provide the best sensing performance.

STATEMENT OF THE PROBLEM

The increasing demand for reliable ethanol gas sensors has stimulated research into the development of advanced nanostructured materials capable of supporting effective gas detection. Although metal oxides such as ZnO, SnO_2 and NiO have attracted considerable attention because of their chemical stability and suitability for gas-sensing applications, their performance can be influenced by limitations associated with surface properties, particle agglomeration and other structural characteristics. Consequently, incorporating metal oxides with reduced graphene oxide (rGO) and gold nanoparticles (AuNPs) offers an opportunity to develop hybrid nanocomposites with potentially improved physicochemical properties for gas-sensing applications.

Despite previous investigations into metal oxide-based nanomaterials, rGO–metal oxide composites and gold nanoparticle–metal oxide systems, there remains a need for comprehensive characterization of hybrid structures combining these three components. In particular, understanding their morphological, elemental, crystalline, chemical and textural properties is essential for establishing their structural characteristics and potential suitability for ethanol sensing. Therefore, this study addresses the need to synthesize and systematically characterize ZnO–rGO–AuNPs, SnO_2–rGO–AuNPs and NiO–rGO–AuNPs hybrid nanocomposites using complementary analytical techniques.

PURPOSE OF THE STUDY

The main purpose of this study was to synthesize and comprehensively characterize ZnO–rGO–AuNPs, SnO_2–rGO–AuNPs and NiO–rGO–AuNPs hybrid nanocomposites to establish their structural, morphological, elemental, chemical and textural properties relevant to their potential application in ethanol gas sensing. Specifically, the study employed field-emission scanning electron microscopy (FESEM), energy-dispersive X-ray spectroscopy (EDX), X-ray diffraction (XRD), Fourier-transform infrared (FTIR) spectroscopy and Brunauer–Emmett–Teller (BET) analysis to investigate the characteristics of the synthesized materials.

INSTRUMENTATION

Field Emission Scanning Electron Microscopy (FESEM)

Field Emission Scanning Electron Microscopy was used to evaluate the produced samples' morphology. A JEOL JSM 7600F with an accelerating voltage of 10.0 kV was used to capture the photos. In order to guaranty conductivity during sample preparation, a thin layer of gold was applied to the surface under high vacuum. After that, carbon tape was used to secure the coated sample to the substrate. The material's surface structure and morphology at the nanoscale were seen in high resolution using FESEM images obtained at magnifications of 50 kx and 100 kx (Kumar and Puri, 2024; Nhiem et al., 2025).

Energy-Dispersive X-ray Spectroscopy (EDX)

The FESEM device (JEOL JSM 7600F) was interfaced with EDX for elemental analysis of the produced nanomaterials. An X-ray beam was focused on certain areas of the sample surface seen in the FESEM pictures during the examination. As a result of this interaction, the atoms' inner-shell electrons are excited and then replaced by electrons from higher energy levels. The elements in the sample can be identified by detecting the distinctive X-rays that are released as a result of the energy difference (Kumar and Puri, 2024; Nhiem et al., 2025).

X-ray Diffraction (XRD) Analysis

XRD techniques were used to investigate the crystallographic characteristics of the produced material. An Xpert Pro PW 3040 with Cu Kα radiation (λ = 1.5406 Å) was used to perform X-ray diffraction for structural analysis, scanning from 20° to 80° in 2θ. The sample was uniformly dispersed on a sample holder and finely ground before the analysis. OriginPro 2024 software was used to analyze and show the obtained diffraction data (Li, 2025).

Fourier Transform Infrared (FTIR) Spectroscopy

The INVENIO FT-IR Spectrometer was used to identify the unique chemical functionalities in the synthesized compounds. Preceding the analysis, the samples were dried thoroughly to minimize the water content. Measurements covered the infrared region from 4000 cm^{-1} down to 400 cm^{-1}, using a resolution setting of 4 cm^{-1}. This technique is based on the interaction of infrared radiation with the sample, resulting in absorption bands that provide a molecular fingerprint corresponding to the vibrational modes of specific chemical bonds (Lim et al., 2024).

Brunauer-Emmett-Teller (BET) Analysis

The Micromeritics TriStar II Plus (USA) system was utilized for BET surface area and pore structure evaluation of the prepared nanocomposite. The analysis was conducted using nitrogen (N_2) adsorption at a bath temperature of -195.8°C. Prior to the measurements, the sample was prepared with a mass of 0.1919 g. Cold free space and warm free space were recorded as 47.8899 cm^3 and 15.3638 cm^3, respectively, with an equilibration interval of 5 s. The porosity characteristics, including total pore volume and pore diameter, were determined using MicroActive software (Nguyen et al., 2026).

RESULTS AND DISCUSSION

FESEM Analysis

The surface morphology of the synthesized ZnO-rGO-AuNPs, SnO_2-rGO-AuNPs, and NiO-rGO-

AuNPs nanocomposites was investigated using field-emission scanning electron microscopy (FESEM). Representative FESEM images recorded at magnifications of 50,000× and 100,000× are presented in Fig. 1. The obtained FESEM images reveal that all samples exhibit nanoscale features distributed over the rGO sheets, with varying degrees of particle agglomeration. The ZnO-rGO-AuNPs nanocomposite shows a highly porous and loosely packed structure composed of relatively finer particles, which is advantageous for gas sensing applications as it facilitates gas diffusion and provides abundant active sites for surface reactions. In comparison, the SnO_2-rGO-AuNPs sample displays a more compact and densely packed morphology, whereas the NiO-rGO-AuNPs nanocomposite presents larger and more aggregated particles, indicating stronger interparticle interactions.

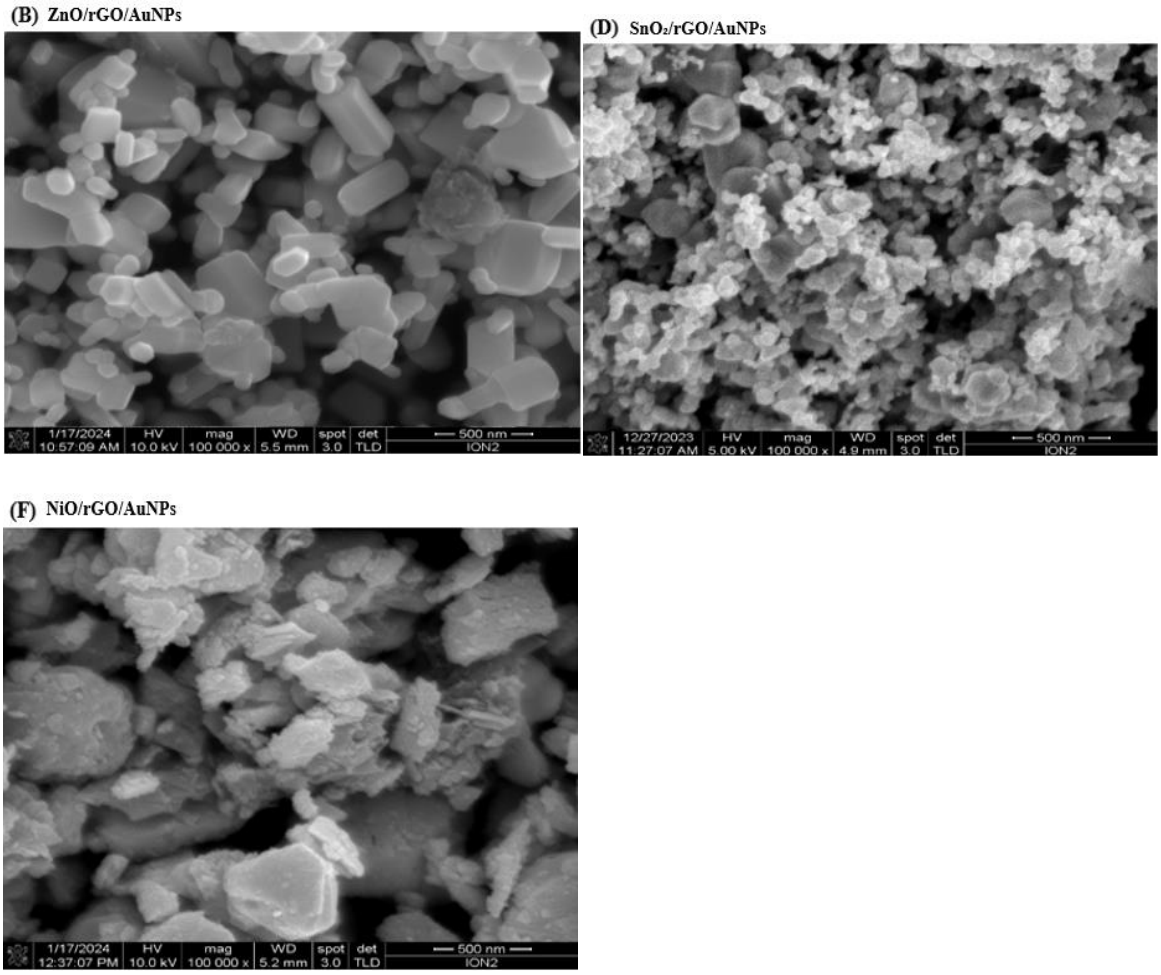

Figure 1: FESEM images of (B) ZnO/rGO/AuNPs, (D) SnO_2/rGO/AuNPs, and (F) NiO/rGO/AuNPs nanocomposites at magnifications of 100,000, respectively.

EDX Analysis

The elemental composition of the synthesized nanocomposites was analyzed using EDX, and the results are presented in Figure 2. For the ZnO-rGO-AuNPs nanocomposite, Zn, O, and C were detected with weight percentages of 66.86%, 20.85%, and 12.29%, respectively, and atomic percentages of 30.54%, 38.91%, and 30.56%. The high weight percentage of Zn confirms that ZnO is the dominant component, while the presence of O corresponds to ZnO and C originates from the rGO support; the slightly higher atomic proportions of O and C relative to Zn are consistent with the molecular structure of ZnO and the contribution of rGO. In the SnO_2-rGO-AuNPs sample, Sn, O, and C were observed with weight percentages of 68.52%, 22.80%, and 7.68%, and atomic percentages of 22.10%, 53.78%, and 24.12%, as shown in Fig. 2B.

The dominance of Sn by weight indicates successful SnO_2 formation, and the higher atomic percentage of O aligns with the Sn:O of 1:2, while C comes from the rGO framework. For NiO-rGO-AuNPs, Ni, O, and C were detected with weight percentages of 65.57%, 21.18%, and 13.25% and atomic percentages of 31.51%, 37.35%, and 31.13%, as illustrated in Fig. 2C. Ni predominates by weight, confirming successful NiO synthesis, O is consistent with NiO formation, and C reflects the rGO support. The nearly balanced atomic percentages in this composite emphasize the significant contribution of rGO in the overall structure. It should be noted that Au peaks were not observed in the EDX spectra. This is likely due to the highly dispersed and possibly embedded nature of the Au nanoparticles within the nanocomposite matrix, which can reduce their detectability in surface-sensitive EDX analysis, even when the overall Au concentration is above the technique's nominal detection limit (~0.08–0.1 wt %) (Vajová et al., 2025). Overall, the EDX results confirm the successful incorporation of the metal oxides onto the rGO/AuNPs support in all three nanocomposites.

(A)

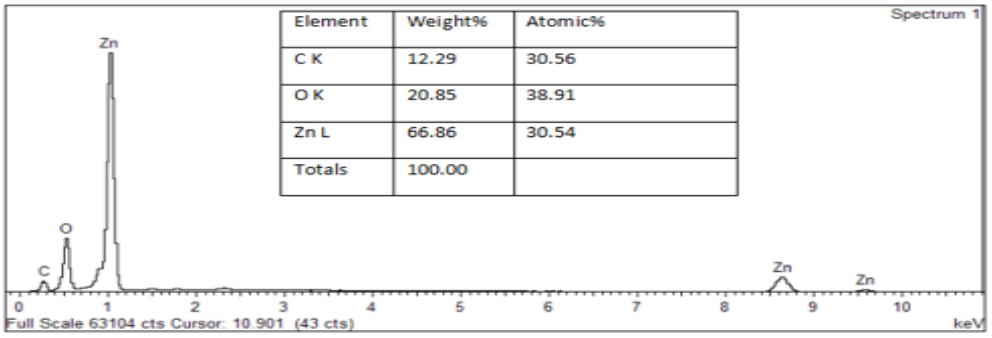

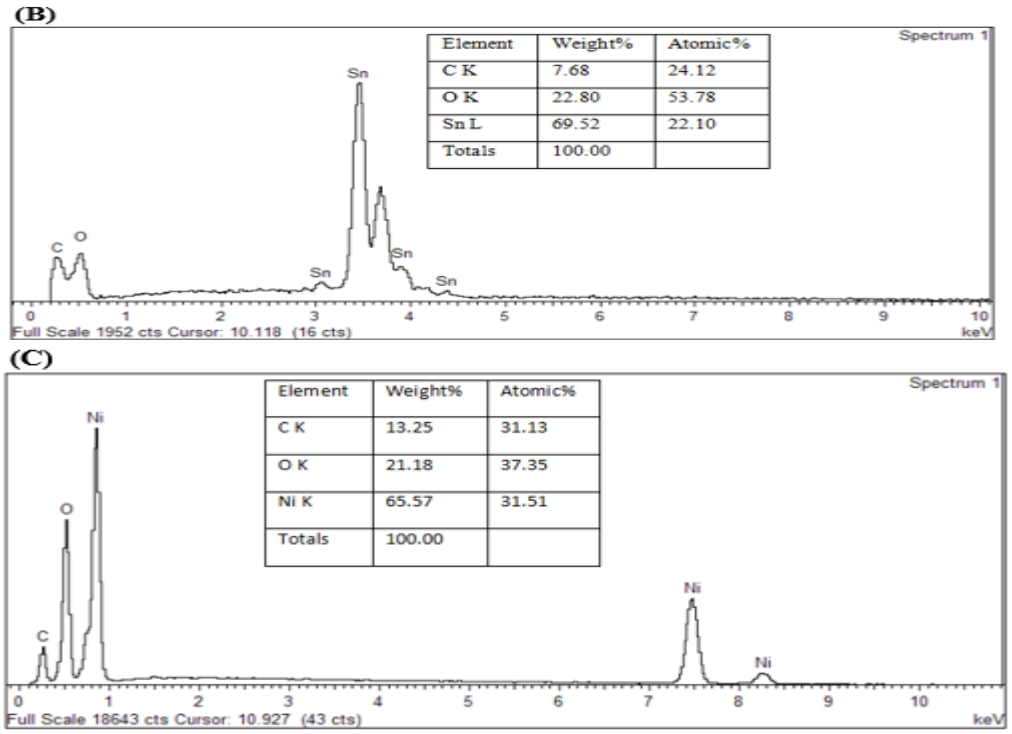

Figure 2: EDX spectra and elemental composition of (a) ZnO/rGO/AuNPs, (b) SnO_2/rGO/AuNPs, (c) NiO/rGO/AuNPs.

XRD Analysis

The crystallinity of the fabricated nanocomposites plays a crucial role in their gas sensing performance, as higher crystallinity improves electron transport and response stability, while defects and surface features can provide additional adsorption sites for gas molecules, enhancing sensitivity and overall performance (Hjiri et al., 2024; Khnykov et al., 2025). The crystallite sizes of the synthesized nanocomposites were estimated using the Scherrer equation:

$$D = \frac{K\lambda}{\beta \cos\ \theta}$$

where $D$is the crystallite size, $K$is the shape factor (0.9), $\lambda$is the X-ray wavelength, $\beta$is the full width at half maximum (FWHM) in radians, and $\theta$is the Bragg angle.

The phase composition and crystallinity of the fabricated nanocomposites were analyzed using X-ray diffraction (XRD). The XRD pattern of the ZnO–rGO–AuNPs nanocomposite (Figure 3A) exhibits well-defined diffraction peaks at 2θ ≈ 31.7°, 34.4°, 36.2°, 47.5°, 56.6°, 62.8°, and 68.0°, which correspond to the (100), (002), (101), (102), (110), (103), and (112) crystallographic planes of hexagonal wurtzite ZnO (JCPDS No. 36-1451) (Anik et al., 2025). The average crystallite size

of ZnO, calculated from the (100) diffraction peak, was approximately 18 nm, suggesting a well-crystallized ZnO nanostructure. Additional diffraction peaks observed at 2θ ≈ 38.2°, 44.4°, 64.6°, and 77.5° are indexed to the (111), (200), (220), and (311) planes of face-centered cubic Au nanoparticles, consistent with previously reported XRD patterns of Au nanostructures (Bibi *et al.*, 2026), and in agreement with the standard data for metallic gold (JCPDS No. 04-0784). Furthermore, a broad diffraction feature centered around 2θ ≈ 25–26° is attributed to the (002) plane of reduced graphene oxide (rGO), reflecting the disordered stacking of graphene layers after reduction, as commonly reported for ZnO/rGO-based nanocomposites (Madi et al., 2024).

The XRD pattern of the SnO_2–rGO–AuNPs nanocomposite (Figure 3B) exhibits distinct diffraction peaks at 2θ ≈ 26.6°, 33.9°, 37.9°, 51.8°, and 54.7°, which are indexed to the (110), (101), (200), (211), and (220) planes of tetragonal SnO_2 (JCPDS No. 41-1445) (Wang et al., 2022). The average crystallite size of SnO_2, calculated from the (110) diffraction peak, was approximately 20 nm, indicating good crystallinity of the SnO_2 phase. In addition, characteristic diffraction peaks corresponding to Au nanoparticles, similar to those observed in the ZnO–rGO–AuNPs nanocomposite, are also present. A broad diffraction feature centered around 2θ ≈ 25–26° is attributed to the (002) plane of reduced graphene oxide (rGO), which partially overlaps with the SnO_2 (110) peak and is commonly reported for SnO_2/rGO-based nanocomposites, supporting the presence of rGO within the composite structure (Alaizeri et al., 2022).

For the NiO–rGO–AuNPs nanocomposite (Figure 3C), a series of diffraction peaks are observed at 2θ ≈ 37°, 43°, 62°, 75°, and 79°, which can be indexed to the (111), (200), (220), (311), and (222) planes of cubic NiO (JCPDS No. 44-1159) (Amir et al., 2025), confirming the formation of the cubic NiO phase. The average crystallite size of NiO, calculated from the (111) diffraction peak, was approximately 17 nm, indicating nanoscale crystallinity of the NiO phase. In addition, diffraction peaks appearing at 2θ ≈ 38°, 44°, 65°, and 77° are attributed to face-centered cubic Au nanoparticles. In contrast to the ZnO–rGO–AuNPs and SnO_2–rGO–AuNPs nanocomposites, the characteristic (002) diffraction feature of reduced graphene oxide (rGO) is significantly weakened or not clearly distinguishable, which is commonly associated with strong interfacial interactions between NiO nanoparticles and rGO sheets that suppress graphene layer restacking (Lateef et al., 2025).

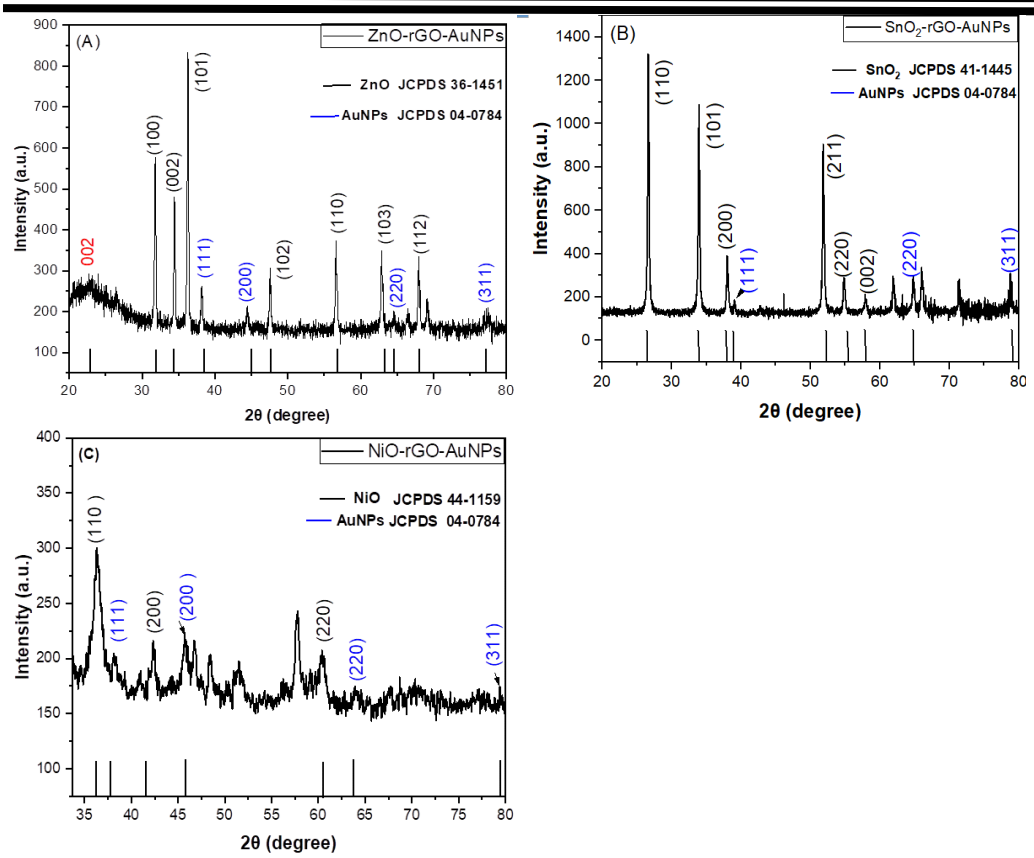

Figure 3: X-ray diffraction (XRD) patterns of (A) ZnO-rGO-AuNPs, (B) SnO_2-rGO-AuNPs, (C) NiO-rGO-AuNPs

FTIR Analysis

The molecular composition and functional groups of the fabricated nanocomposites were analyzed using Fourier Transform Infrared (FTIR) spectroscopy, as shown in Figure 4. A broad peak around 3400 cm^{-1} in all samples corresponds to O–H stretching vibrations of hydroxyl groups, commonly present on the surface of reduced graphene oxide (rGO) due to incomplete reduction, leaving residual oxygen-containing groups (Popov *et al.*, 2021). A peak near 1600–1650 cm^{-1} observed in all the composites corresponds to C=C stretching vibrations, indicating the presence of graphitic domains in the material (Hussain et al., 2022). In the ZnO–rGO–AuNPs nanocomposite, an absorption band observed at approximately 500 cm^{-1} is assigned to Zn–O stretching vibrations (Samuel et al., 2025). For the SnO_2–rGO–AuNPs nanocomposite, a sharp band appearing at around 610 cm^{-1} corresponds to Sn–O stretching vibrations, while in the NiO–rGO–AuNPs nanocomposite, a distinct absorption peak at approximately 511 cm^{-1} is attributed to Ni–O stretching vibrations (Verma et al., 2025; Zeyrek Ongun & Oguzlar, 2023). Weak bands near 2350–2400 cm^{-1} in the SnO_2–rGO–AuNPs spectrum are attributed to CO_2 asymmetric stretching,

likely from surface adsorption or the measurement environment (Madi et al., 2024). Thus, the FTIR results confirm the successful synthesis of ZnO, SnO_2, and NiO nanostructures and the presence of their characteristic functional groups in the nanocomposites.

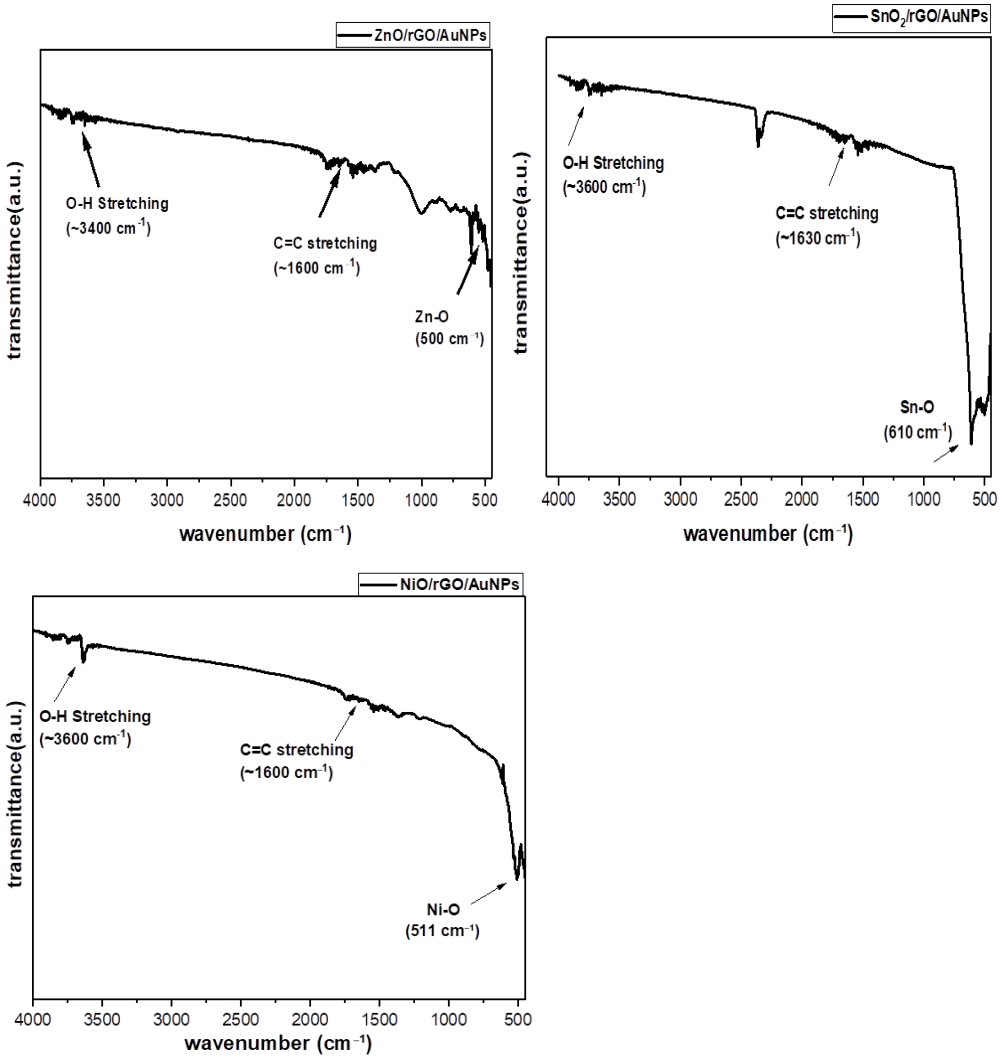

Figure 4: FTIR spectra for (A) ZnO-rGO-AuNPs, (B) SnO_2-rGO-AuNPs, (C) NiO-rGO-AuNPs.

BET Analysis

BET and BJH surface analyses were employed to evaluate the specific surface area and porosity of the synthesized nanocomposites. The N_2 adsorption–desorption isotherms and corresponding pore size distribution curves of the ZnO–rGO–AuNPs, SnO_2–rGO–AuNPs, and NiO–rGO–AuNPs nanocomposites (Fig. 5) exhibit Type IV behavior with H3 hysteresis loops, indicating multilayer

adsorption and the presence of slit-like mesopores formed by aggregates of plate-like particles, according to the IUPAC classification of physisorption isotherms (Sing et al., 2024).

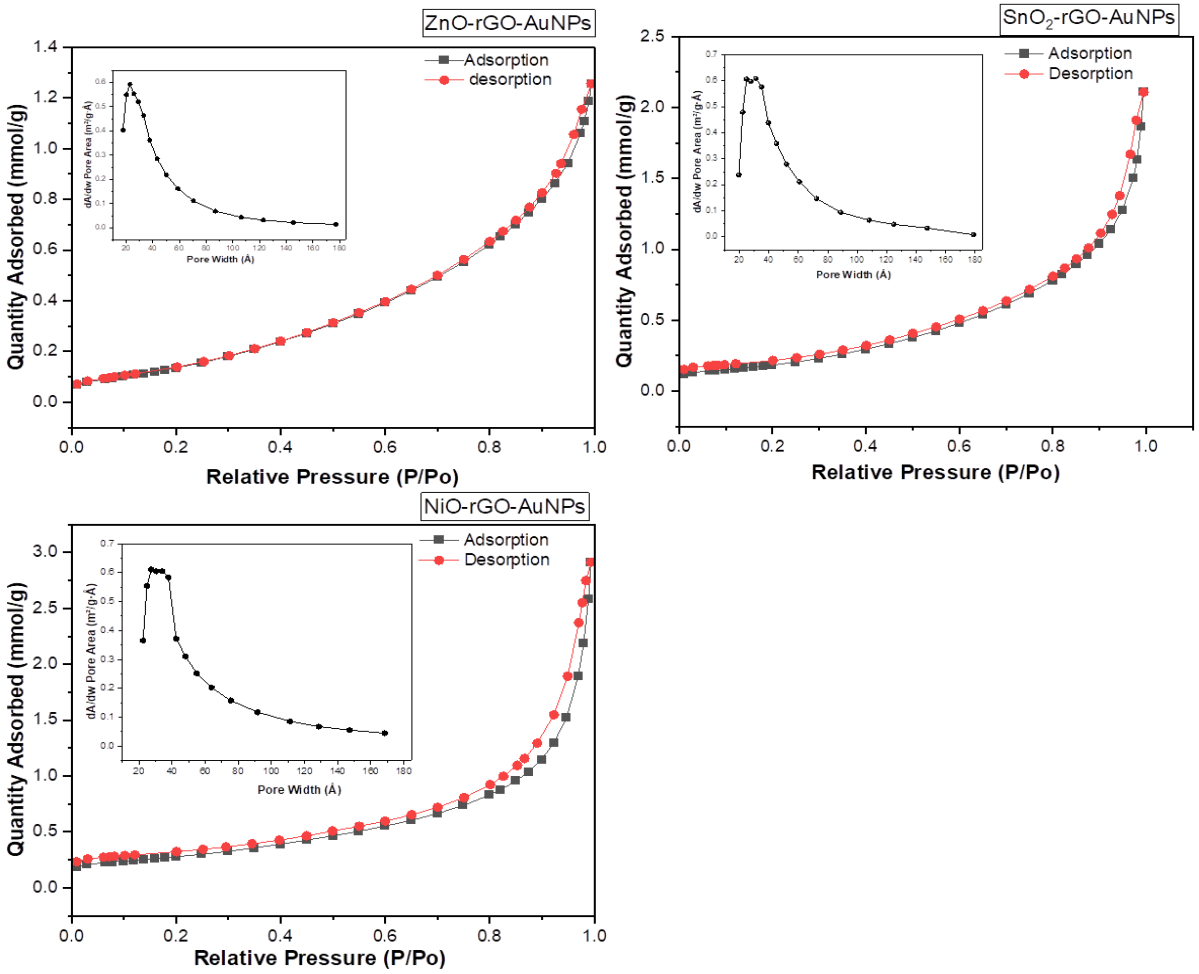

Figure 5: N_2 adsorption–desorption isotherms and BJH pore size distribution curves for (A) ZnO–rGO–Au hybrids, (B) SnO_2–rGO–Au hybrids, and (C) NiO–rGO–Au nanocomposites.

TABLE 1: BET SURFACE AREA, PORE VOLUME, AND PORE SIZE OF ZNO–RGO–AU, SNO_2–RGO–AU, AND NIO–RGO–AU NANOCOMPOSITES

Sample	BET Surface Area (m^2/g)	Pore Volume (cm^3/g)	Average Pore Diameter (nm)
ZnO/rGO/AuNPs	12.42	0.0287	5.18
SnO_2/rGO/AuNPs	16.16	0.0383	5.59
NiO/rGO/AuNPs	22.28	0.0471	6.50

CONCLUSION

The study successfully demonstrated the synthesis and characterization of hybrid nanocomposites based on metal oxides (ZnO, SnO_2, and NiO), reduced graphene oxide (rGO), and gold nanoparticles (AuNPs). The nanocomposites were synthesized via a simple and hydrothermal method, which can be adapted, aiming to overcome the limitations of conventional metal-oxide gas sensors, particularly high operating temperature, poor selectivity, and high-power consumption.

Comprehensive structural and physicochemical characterization using XRD, FESEM, EDX, FTIR, and BET analyses confirmed the successful possible formation of metal oxide–rGO–AuNP hybrid structures. XRD results verified the crystalline phases of ZnO, SnO_2, and NiO along with the presence of rGO and AuNPs, while FESEM images revealed nanoscale morphologies with varying degrees of porosity and particle agglomeration. BET analysis indicated mesoporous structures for all nanocomposites, which are favorable for gas diffusion and surface reactions.

SUGGESTIONS

Based on the findings of this study, the following suggestions are made:

1. Further studies should employ complementary analytical techniques, such as TEM and XPS, to provide additional evidence of the incorporation and distribution of Au nanoparticles in the hybrid nanocomposites.

2. Experimental ethanol gas-sensing tests should be conducted to establish the sensitivity, selectivity, response and recovery times, and stability of the synthesized materials.

3. Further investigations should examine how synthesis conditions and component concentrations influence the structural, morphological and textural properties of the nanocomposites.

4. Comparative studies should evaluate the suitability of the three nanocomposites for ethanol gas-sensing applications under controlled experimental conditions.

REFERENCES

Abdelghani, R. M., Kashyout, A. E. H. B., Morsi, I., Taha, T. E., Soliman, N. F., & El-Shafai, W. (2025). Synthesis and characterization of hematite nanomaterials imprinted with acetone, ethanol and methanol for AI-Based IoT gas sensor arrays. *Scientific Reports*, *15*(1), 29821. https://doi.org/10.1038/s41598-025-06724-0

Alaizeri, Z. M., Alhadlaq, H. A., Aldawood, S., Akhtar, M. J., & Ahamed, M. (2022). One-Pot Synthesis of SnO_2-rGO Nanocomposite for Enhanced Photocatalytic and Anticancer Activity. *Polymers*, *14*(10). https://doi.org/10.3390/polym14102036

Amir, J., Muhammad, S., Kashif, M., Khan, A. A., Gul, M., Sun, H., Shah, M., Azizi, S., & Maaza, M. (2025). Synthesis, characterization and dielectric properties evaluation of NiO-CO_3O_4 nanocomposite. *Journal of the Iranian Chemical Society*, *22*(1), 63–72. https://doi.org/10.1007/s13738-024-03129-0

Anik, A. B., Hossen Akash, M., Alam, M. A., Alam, M. Z., Sarker, D., & Sultana, N. (2025). Green synthesis of ZnO nanoparticles using Justicia adhatoda for effective photocatalytic degradation of methylene blue dye. *RSC Advances*, *15*(54), 45874–45888. https://doi.org/10.1039/d5ra06656e

Bibi, Y., Nasreen, Z., Gul, H., Assad, N., Khan, M. N., Kifle, D., Naeem-Ul-Hassan, M., & Ercişli, S. (2026). Phytosynthesis of gold nanoparticles from Boerhavia diffusa L. and their antibacterial, antifungal, antioxidant, and anticancer activities. *Discover Nano*, *21*(1), 7. https://doi.org/10.1186/s11671-025-04425-1

Enferadi, S. M. H. B., & Mirzaei, A. (2024). Fe2O3-Co3O4 nanocomposite gas sensor for ethanol sensing studies. *Ceramics International*, *50*(24), 52861-52870. https://doi.org/10.1016/j.ceramint.2024.10.138

Gambhire, M. S., Labhade, S. R., Gaikwad, S. S., & Shaikh, S. A. (2026). Synthesis and development of polyaniline-manganese dioxide composite thick films for acute detection of ethanol gas. *Journal of the Indian Chemical Society*, **103**, 102450. http//doi.org/10.1016/j.jics.2026.102450.

Godja, N.-C., & Munteanu, F.-D. (2024). Hybrid Nanomaterials: A Brief Overview of Versatile Solutions for Sensor Technology in Healthcare and Environmental Applications. *Biosensors*, *14*(2), 67. https://doi.org/10.3390/bios14020067

Hussain, T., Ahmad, K., Mujahid, A., Afzal, A., & Abbas, U. (2022). Physiochemical Modification of Graphene Nanosheets to tailor Electrical Properties of Graphene based PMMA Composites. In *Journal of Materials and Electronic Devices* (Vol. 4) 1, 40 - 44.

Kumar, S., & Puri, N. K. (2024). Highly selective sustainable ethanol gas sensor based on pp heterojunction of SnS/MoSe2 nanocomposite at room temperature. *Materials Chemistry and Physics*, *326*, 129802. https://doi.org/10.1016/j.matchemphys.2024.129802

Lateef, R., Marhaba, Anjum, S., Ansari, K. M., Ahmad, I., Lohia, N., Alhadlaq, H. A., Akhtar, M. J., & Ahamed, M. (2025). NiO@rGO nanohybrids triggered cytotoxicity via oxidative stress, cell cycle arrest, and apoptosis pathways. *Scientific Reports*, *15*(1). https://doi.org/10.1038/s41598-025-07131-1

Li, X. (2025). Preparation of porous flower-like graded structure Co3O4/g-C3N4 and its ethanol gas-sensitive properties. *Main Group Chemistry*, *24*(2), 107-116. https://doi.org/10.1177/10241221251321827

Li, G., Hou, J., Hilal, M., Kim, H., Chen, Z., Cui, Y., Kim, J. H., & Cai, Z. (2024). Development of High-Performance Ethanol Gas Sensors Based on La2O3 Nanoparticles-Embedded Porous SnO2 Nanofibers. *Sensors*, *24*(21). https://doi.org/10.3390/s24216839

Lim, H., Kwon, H., Kang, H., Jang, J. E., & Kwon, H. J. (2024). Laser-induced and MOF-derived metal oxide/carbon composite for synergistically improved ethanol sensing at room temperature. *Nano-Micro Letters*, *16*(1), 113. https://doi.org/10.1007/s40820-024-01332-5

Machín, A., & Márquez, F. (2025). Next-generation chemical sensors: The convergence of nanomaterials, advanced characterization, and real-world applications. *Chemosensors*, *13*(9), 345. https://www.mdpi.com/2227-9040/13/9/345

Madi, K., Chebli, D., Ait Youcef, H., Tahraoui, H., Bouguettoucha, A., Kebir, M., Zhang, J., & Amrane, A. (2024a). Green Fabrication of ZnO Nanoparticles and ZnO/rGO Nanocomposites from Algerian Date Syrup Extract: Synthesis, Characterization, and Augmented Photocatalytic Efficiency in Methylene Blue Degradation. *Catalysts*, *14*(1). https://doi.org/10.3390/catal14010062

Nagar, R., & Kamathe, V. (2024). Efficient Room Temperature Ethanol Vapor Sensing by Unique Fractal Features of Tin Oxide. *Igmin Research*, *2*(2), 097-101. https://dx.doi.org/10.61927/igmin150

Nguyen, H. M., Cao, P. V., Cao, A. V., Nguyen, H. M., Nguyen, C. D., Vu, T. H., ... & Kim, D. (2026). Arc-discharge-assembled CNT/MoO3 nanohybrids for ultra-sensitive and selective sub-ppm ethanol detection at room temperature. *RSC advances*, *16*(17), 15464-15476. https://doi.org/10.1039/d6ra00372a

Nhiem, L. T., Mao, J., Ta, Q. T. H. & Seo, S. (2025). "Highly selective ethanol gas sensor based on CdS/$Ti_3C_2T_x$ MXene composites." *Nanoscale Advances*, 7, 1452–1463. http//doi.org/ 10.1039/D4NA00927D

Popov, A., Aukstakojyte, R., Gaidukevic, J., Lisyte, V., Kausaite-Minkstimiene, A., Barkauskas, J., & Ramanaviciene, A. (2021). Reduced graphene oxide and polyaniline nanofibers nanocomposite for the development of an amperometric glucose biosensor. *Sensors (Switzerland)*, *21*(3), 1–15. https://doi.org/10.3390/s21030948

Ranga, J., Kumar, S. S., Ketaraju, V. D. S., Maroor, J. P., Kolikipogu, R., & Gopinath, D. (2026). Room-temperature methanol sensing using PEDOT: PSS–WO_3 hybrid nanocomposites with enhanced sensitivity and fast response. *Journal of Porous Materials*, *33*(1), 267-278.

https://doi.org/10.1007/s10934-025-01869-9

Samuel, A., Abdullah, A., Xavier, G., Stephen, S., Zeidan, M. M., Choi, D., & Abedrabbo, S. (2025). Sol-gel synthesis and characterization of ZnO-SiO_2 nanocomposites: a comparative study with pure ZnO and SiO2. *Nanoscale Advances*. https://doi.org/10.1039/d5na00612k

Shah, A. H., Anas, M., Alomar, M., Hanif, M., Zubair, M., & ur Rehman, N. (2025). Ultra-fast real time ethanol sensing behavior and reduction in optical bandgap of the hydrothermally synthesized V2O5/ZnO nanocomposites. *Chemical Physics Impact*, *10*, 100879. https://doi.org/10.1016/j.chphi.2025.100879

Singh, S., Bhardwaj, S., Tiwari, P., Dev, K., Ghosh, K., & Maji, P. K. (2024). Recent advances in cellulose nanocrystals-based sensors: a review. In *Materials Advances* (Vol. 5, Number 7, pp. 2622–2654). Royal Society of Chemistry. https://doi.org/10.1039/d3ma00601h

Suresh, V., Nagaraju, P., Kathirvelu, V., Parne, S. R., & Jeyaselan, J. J. J. (2026). Synthesis and characterization of ZnO and ZnO–MoO_3 composite thin films ethanol detection. *Next Materials*, *13*, 102961. https://doi.org/10.1016/j.nxmate.2026.102961

Tian, Y., Wang, J., Wang, J., et al. (2026). High-performance ethanol gas sensor based on stepped and hollow $ZnSnO_3$/Co_3O_4 heterostructures. *Chemical Engineering Journal*, 174092. http//doi.org/ 10.1016/j.cej.2026.174092.

Vajová, I., Vizárová, K., Tiňo, R., Králik, M., Nosko, M., Múčka, P., Rudinská, D., & Katuščák, S. (2025). Choosing between energy-dispersive or wavelength-dispersive SEM spectroscopy methods for elemental distribution in deacidified paper. *Cellulose*, *32*(16), 9231–9243. https://doi.org/10.1007/s10570-025-06771-w

Verma, B., Kumar, A., Swart, H. C., & Kumar, V. (2025). Enhanced optical and electrical properties of NiO-GO composite thin films on flexible PET substrates for optoelectronic applications. *Chemistry of Inorganic Materials*, *5*, 100097. https://doi.org/10.1016/j.cinorg.2025.100097

Wan, Y., Liu, Y., Huang, Y., Zhao, L., Lu, H. L., & Gao, L. (2026). Au-decorated NiO/ZnO nanoflowers for ultra-fast and selective ethanol sensing. *Journal of Alloys and Compounds*, 187645. https://doi.org/10.1016/j.jallcom.2026.187645

Wang, C., Guo, G., Zhu, C., Li, Y., Jin, Y., Zou, B., He, H., & Wang, A. (2022). Facile Synthesis, Characterization, and Photocatalytic Evaluation of In_2O_3/SnO_2 Microsphere Photocatalyst for Efficient Degradation of Rhodamine B. *Nanomaterials*, *12*(18). https://doi.org/10.3390/nano12183151

Zeyrek Ongun, M., & Oguzlar, S. (2023). Improvement of the CO_2 Sensitivity: HPTS-Based Sensors along with Zn@SnO_2 and Sn@ZnO Additives. *ACS Omega*, *8*(32), 29635–

29645. https://doi.org/10.1021/acsomega.3c03708